Charles University in Prague
Faculty of Mathematics and Physics

Summary of doctoral thesis

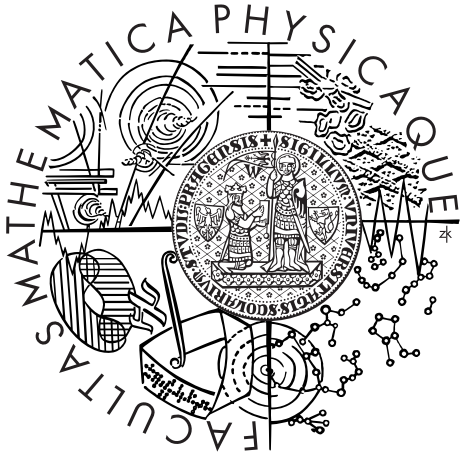

Nina Benešová

Thermal Convection in Terrestrial Planetary Mantles

Department of Geophysics

Supervisor of the doctoral thesis: Doc. RNDr. Hana Čížková PhD.
Study programme: Physics
Specialization: Geophysics

Prague 2015

Univerzita Karlova v Praze
Matematicko-fyzikální fakulta

Autoreferát disertační práce

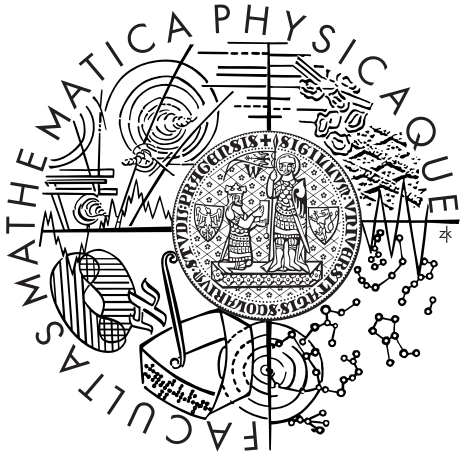

Nina Benešová

Termální konvekce v pláštích terestrických těles

Katedra geofyziky

Vedoucí disertační práce: Doc. RNDr. Hana Čížková PhD.

Studijní program: Fyzika

Studijní obor: Geofyzika

Praha 2015

Dizertace byla vypracována na základě výsledků získaných v letech 2008–2012 během doktorandského studia na Katedře geofyziky MFF UK.

Dizertant:
Mgr. Nina Benešová
Katedra geofyziky MFF UK
V Holešovičkách 2, 180 00 Praha 8

Školitel:
Doc. RNDr. Hana Čížková, Ph.D.
Katedra geofyziky MFF UK
V Holešovičkách 2, 180 00 Praha 8

Oponenti:
RNDr. Pavel Hejda CSc.
Geofyzikální ústav AV ČR
Boční II/1401, 141 31 Praha 4

RNDr. Ondřej Šrámek, Ph.D.
Katedra geofyziky MFF UK
V Holešovičkách 2, 180 00 Praha 8

Předseda oborové rady:
Doc. RNDr. Hana Čížková, Ph.D.
Katedra geofyziky MFF UK
V Holešovičkách 2, 180 00, Praha 8

Obhajoba dizertace se koná dne 9. září 2015 v 10 hodin před komisí pro obhajoby dizertačních prací v oboru Geofyzika v budově MFF UK, Ke Karlovu 3, Praha 2, v místnosti M252.

S dizertací je možno se seznámit v PGS MFF UK, Ke Karlovu 3, Praha 2.

Contents

Introduction

The terrestrial bodies have a similar composition and structure as our Earth. They are assumed to have formed through the same processes of accretion and differentiation. They have a solid surface, they are composed mainly of silicate rocks and metals and they have the same structure of a metallic (mostly iron) core inside a silicate mantle. Those bodies can be planets (including exoplanets) or smaller bodies like satellites of the planets (e.g. the Moon). In the Solar System, there are four terrestrial planets: Mercury, Venus, Earth and Mars.

Although those terrestrial planets are similar in some basic characteristics, they differ in many ways. Among other things, Earth is the only planet where the surface plate motion is currently observed. It has been widely accepted that the primary mechanism that can explain its internal dynamics is mantle convection as, on the geological time scale, the mantle material flows as a viscous fluid. The energy driving the convection originates from primordial heat and from a decay of radioactive elements. This energy is manifested on the surface by the plate tectonics. Other planets do not reveal their internal dynamics in such a way and we have only indirect information about their internal processes. Therefore, it is difficult to determine whether these planets experience thermal convection at present. It is assumed that these planets must transfer heat from the core to the surface in a similar

fashion as the Earth, and that they experienced mantle convection at least in the past, although its regime might have been different.

Various approaches can be used for constraining the structure and the internal dynamics of the Earth and other planets. An inversion of the seismic data (travel times, waveforms, free-oscillations) provides rather detailed information about the structure of the Earth interior. However, it provides only a snapshot of the present state, moreover, it is not available for other planets.

That is why numerical simulations of mantle convection are traditionally used to investigate thermal evolution and dynamical processes in the mantle. Character of the convection is determined by the parameters of the mantle material (viscosity, thermal expansivity, thermal diffusivity, etc.). With increasing pressure and temperature, the material undergoes mineralogical changes and its properties can change considerably. The deformation of mantle rocks under the conditions of the Earth's deep interior can be studied by laboratory experiments and ab initio calculations. Both approaches give crucial constraints on mantle material properties. However, they have large uncertainties and give only a range of possible values. Mantle convection models can be then used to put additional constraints on those parameters. We can use numerical models to explore the parameter space by running multiple calculations with varying input parameters. Then we can compare the output with the observed quantities (e.g. heat flow, character of thermal anomalies, gravity, topography, etc.) and thus we can identify the admissible models satisfying the observations.

High demands on computational capacities is a restraining factor in using numerical models. Since the field of computer technology is developing rapidly it becomes more and more feasible to perform calculations in a realistic 3D spherical geometry. Nevertheless, it is still computationally challenging to carry out the simulations with realistic material characteristics and complex mantle processes. This explains the common use of simplifying geometries like cylindrical, spherical axisymmetric or Cartesian. Within the scope of this work, a convection code was developed, which allows to carry out the calculations both in axisymmetric spherical shell and in fully 3D spherical geometry with some additional simplifying assumptions to reduce the computational costs. The code was applied to problems related to Venus, Mercury and Earth mantle evolution.

From all the terrestrial planets, Venus most closely resembles the Earth and it is sometimes called Earth's sister planet. It has similar size, mass, surface composition and distance to the Sun. On the other hand, it is markedly different in other aspects. It has a dense atmosphere consisting mainly of carbon dioxide that through the greenhouse effect makes Venus the hottest

planet in the Solar System ($\sim$ 735 K at the surface). This thick atmosphere also prevented any visual observations of Venus' surface until the development of radar observations. The surface is shaped by a volcanic activity and no evidences for the plate tectonics were found. In the absence of global tectonics, Venus is often assumed to have a stiff lithosphere that reduces the heat loss from the interior, causing the interior to be relatively hot. This concept could be consistent with the fact that Venus lacks internal magnetic field and it may imply that Venus' heat budget and convective regime are markedly different than the Earth's ones.

Of the Solar System planets, Mercury is the smallest and the closest to the Sun. It is probably the least understood one of the inner planets. Its proximity to the Sun makes it difficult target for both ground-based observations and spacecraft missions. Our knowledge of the planet is based mainly on the measurements made by two spacecraft. Mariner 10 in 1970s provided first close-up images of its surface which revealed its old heavily cratered surface. Recently, our knowledge about the planet was dramatically improved by measurements of MESSENGER mission. Among others, it provided images of the surface in much higher resolution, it was equipped with magnetometer that confirmed the existence of internal magnetic field and its spectrometers provided an estimate of the surface element abundances. Important piece of knowledge is the fact that Mercury has a relatively large core and a thin mantle (in comparison with the other terrestrial planets). This implies that its formation or its evolution may be significantly different from the other planets. Important question arises, whether a viable mantle convection can still occur in such a thin mantle (400 km at maximum).

In the lack of seismic data, an important source of information about internal structure of a planet is its gravity and its topography. The gravitational field of a planet can be constructed through an analysis of the tracking data of an orbiter. The surface topography can be measured from the orbit using a radar altimeter. That data is available for both Venus and Mercury, although their limited resolution and accuracy should be kept in mind. In the case of Venus, gravity and topography data are available with a relatively high resolution based mainly on Pioneer Venus (late 1970s) and Magellan (1990s) measurements. In recent years, these data have been already analysed to reveal some information about the Venusian mantle structure mostly in the terms of steady-state models. Here, we perform a broad parametric study: we vary the viscosity model and the characteristic density distribution (as controlled by Rayleigh number) and we perform time-dependent calculations of thermal convection. Then, we analyse the spectra of the geoid and the topography generated by these models and we compare them to the observed quantities with the aim to constrain the mantle viscosity stratifi-

cation. In the case of Mercury, MESSENGER measurements of gravity and topography are very recent and only few analyses were published so far. We focus here on the main question whether the data is consistent with mantle convection still operating in Mercurian mantle and whether the dynamic support is a possible mechanism that may explain topographic and geoid data.

The last question addressed in this thesis concerns the long-term evolution/ cooling of the Earth mantle. After its formation, $\sim$ 4.5 Ga ago, the Earth was much hotter then nowadays. Since then, it is losing heat primarily by the process of mantle convection. Although the radioactive decay acts as a contrary process (it heats the planet), in total, Earth losses heat and thus cools in time. This process of secular cooling is generally very complex and it depends on the initial state of the Earth on the onset of mantle convection and on the Earth material parameters. The question of Earth cooling has already been addressed in numerous studies and effects of various mantle parameters were investigated. A decade ago a new high-pressure phase of perovskite (post-perovskite) was discovered in the lowermost mantle. It was suggested it has different properties than perovskite (e.g. lower viscosity). Such a distinct layer just above the core-mantle boundary (in mantle convection thermal boundary layer) should exert a significant influence on the cooling process. We study this effect in mantle convection models in combination with the effects of other material parameters.

The structure of the thesis is as follows. Chapter 1 gives an overview of the mathematical description of mantle convection, solution methods and benchmark tests. The results are then divided into two parts. Part I (Chapters 2 and 3) deals with Venus and Mercury and it uses their gravity and topography to constrain their structure and dynamics. Part II (Chapters 4 and 5) focuses on the effects of post-perovskite on the long-term evolution of the Earth and on the possible constraints on its spatial distribution. Appendix introduces the formalism of spherical harmonic functions employed to solve the problem.

Theory and Method

Thermal convection in the mantle is described by the set of equations based on general laws of conservation. Various simplifying approximations and assumptions are usually applied when solving the equations. The extended Boussinesq approximation is used here, which is widely used when simulating mantle convection (e.g. Ita and King, 1994; Matyska and Yuen, 2007; King et al., 2010).

The basic equations in the extended Boussinesq approximation are as follows:

$$\nabla \cdot \boldsymbol{v} = 0, \tag{1}$$

$$\nabla \cdot \tau = -\Delta\varrho\, \boldsymbol{g}, \tag{2}$$

$$\varrho_0 c_p \frac{\partial T}{\partial t} = \nabla \cdot (k\nabla T) - \varrho_0 c_p \boldsymbol{v} \cdot \nabla T - \varrho_0 v_r \alpha T g + \sigma : \nabla \boldsymbol{v} + H + L_t. \tag{3}$$

Eq. (1) is the equation of continuity under the assumption that the material is incompressible. Eq. (2) is the momentum equation assuming the infinite Prandtl number (neglecting inertial forces) and omitting the self-gravitation. Right-hand side (RHS) of this equation is a source term — buoyancy force caused by density heterogeneities. Finally, (3) is the energy equation. Terms on the RHS of the energy equation represent heat conduction, heat advection, adiabatic cooling or heating, viscous dissipation, radioactive heat sources and latent heat associated with phase transitions, respectively. The law of angular momentum conservation further yields that stress tensor τ is a symmetric tensor. For a summary of used symbols see Table 1.

Further, we need to specify the rheological description of the material in terms of constitutive equation — we assume Newtonian fluid:

$$\tau = -pI + \eta\big(\nabla \boldsymbol{v} + (\nabla \boldsymbol{v})^T\big). \tag{4}$$

Here viscosity η can generally be a function of radius (pressure), temperature and mineral phase parametrised by phase function Γ_k (van Hunen, 2001) — $\eta = \eta(r, T, \Gamma_k)$. We assume linearised equation of state with density anomalies depending linearly on temperature variations through thermal expansivity. Equation of state also includes density changes due to phase transitions:

$$\Delta\varrho = -\varrho_0 \alpha (T - T_{ref}) + \sum_k \Delta\varrho_k \Gamma_k. \tag{5}$$

Reference density ϱ_0, gravity acceleration g and specific heat c_p are assumed constant. Expansivity α and thermal conductivity k may generally depend on radius.

The set of equations (1)-(5) has to be supplemented by the boundary conditions. The equations are solved on the domain restricted by two spherical surfaces, the planet's surface and the core-mantle boundary (CMB). On both boundaries impermeable free-slip conditions are prescribed — zero radial velocity:

$$\boldsymbol{v} \cdot \boldsymbol{e}_r = 0 \tag{6}$$

and zero tangential stress:

$$\tau \cdot \boldsymbol{e}_r - ((\tau \cdot \boldsymbol{e}_r) \cdot \boldsymbol{e}_r)\boldsymbol{e}_r = 0. \tag{7}$$

Table 1: Used symbols

$\boldsymbol{v}$	velocity
v_r	radial component of velocity
τ	stress tensor
σ	deviatoric part of the stress tensor
$\boldsymbol{g}$	vector of the gravity acceleration
g	gravity acceleration
t	time
c_p	specific heat at constant pressure
T	temperature
k	thermal conductivity
α	coefficient of thermal expansivity, α_0 denotes reference value
κ	thermal diffusivity ($\kappa = k/\varrho_0 c_p$), κ_0 denotes reference value
H	volume heat sources
L_t	latent heat due to phase changes
p	dynamic pressure
I	identity tensor
η	dynamic viscosity, η_0 denotes reference value
ϱ	density
ϱ_0	reference density at reference temperature T_{ref}
$\Delta\varrho$	density anomalies
Γ_k	phase function of the k-th phase transition
$\Delta\varrho_k$	density change due to the k-th phase transition
T_{top}	temperature at the surface (r_{top})
d	thickness of the mantle
T_{cmb}	temperature at the core-mantle boundary (r_{cmb})
Ra	Rayleigh number
$\boldsymbol{e}_r$	unit radial vector

Further, we prescribe temperatures on both boundaries. Temperatures T_{top} at the surface and T_{cmb} at the core-mantle boundary are constant along the boundary, but T_{cmb} may vary with time in some applications.

The vigour of convection depends on the mantle parameters whose joint influence can be characterised by a single dimensionless parameter — the Rayleigh number:

$$Ra = \frac{\varrho_0 \alpha_0 g (T_{cmb} - T_{top}) d^3}{\kappa_0 \eta_0}. \tag{8}$$

The problem introduced above was solved in spherical geometry. Our solution method is based on spectral decomposition in angular coordinates and finite differences in radial direction (Čížková and Čadek, 1997). We solved the problem both in 2D axisymmetric and fully 3D geometry. In the case of 3D geometry, additional simplifying assumptions were applied (e.g. viscous heating term in energy equation is omitted or only radial dependent viscosity is considered) to reduce computational costs. To verify the performance of developed code several benchmark tests were performed.

Part I: Geoid, Topography and Mantle Convection in Terrestrial Planets — application to Venus

As a sister planet of the Earth, whose dynamic processes should be controlled by the same physical processes, Venus has received a lot of attention from the mantle convection modellers (e.g. Tackley, 1993; Armann and Tackley, 2010). As we have no direct information about the internal structure of the Venus' mantle, the most important data that could constrain mantle processes are the surface topography and the geoid. Numerous studies have used this observation to constrain the mechanisms that maintain the topographic features. The possible mechanisms include isostasy, elastic flexure and mantle flow induced by density. Pauer et al. (2006) have performed the geodynamic inversion of the geoid and topography data in order to estimate the viscosity stratification of the Venus' mantle. Using a rather simplifying assumption, namely that the mass anomaly distribution does not vary with depth, they concluded, that the geoid and topography spectra between the degrees 2 and 40 can be well explained by a whole mantle flow model. One of their best fitting five-layer viscosity profiles has a relatively high-viscosity lithosphere (about 2 orders of magnitude difference with respect to the upper mantle) and shows a gradual increase of viscosity with depth by a factor of 40 in the underlying mantle.

Since the early nineties, the relationship between the topography and the geoid has been studied in the framework of the numerical models of thermal convection in the Venus' mantle. The regional scale models of a single plume were used to put the first constraints on the mantle viscosity distribution on Venus. E.g. Kiefer and Hager (1991) tried to fit the geoid and topography of four selected plumes in a model with a depth dependent viscosity and concluded that their preferred model shows a moderate increase of viscosity in the lower mantle. Solomatov and Moresi (1996) studied the effect of temperature dependent viscosity on the plume evolution and in a Cartesian model. They needed a rather thick lithosphere (200–400 km) to predict an average observed GTR and, for some plume regions, their stagnant lid was as thick as 500 km. Their preferred model was characterized by the Ra of $3{\cdot}10^7$.

Though efficient, the Cartesian or cylindric models of a single plume may suffer from incorrect geometry. It has been pointed out by King (1997) that the predicted geoid could vary by about 50% among the different model geometries (cylindrical, Cartesian and spherical axisymmetric). Therefore the spherical models — axisymmetric or even fully 3D are important in interpreting the geoid and topography data. Another advantage of these global models is the interaction of the plumes with the background mantle flow and a smaller dependence on the initial conditions.

Viscosity is clearly the key parameter controlling the dynamic regime of the mantle, number of plumes etc., and is crucial for understanding the relationship between the dynamic topography and the geoid. This relationship is studied systematically here, in a large group of models with various viscosity profiles and varying several other flow model parameters. Using 3D spherical simulations of thermal convection in a model with depth-dependent viscosity it is tested whether the spectra of our predicted geoid and topography correspond to the observed ones. The results obtained for convection runs with different viscosity profiles are compared here and the effect of Rayleigh number is tested. Besides of the fit of the spectra, the characteristic flow patterns (namely the number of plumes developed) are also compared. Further, in a 2D spherical axisymmetric model, the effect of lateral viscosity variations and internal heating is studied.

In the 2D models, we further evaluate the evolution of the plumes and compare their geoid and topography signature with the observations at selected upwelling structures on Venus. We compared the shape of the geoid and the topography anomaly above the plume developed on the pole of our 2D axisymmetric model with several topographic rises on Venus. About dozen of the Venus' rises are often interpreted by underlying thermal upwellings (Stofan and Smrekar, 2005; Smrekar et al., 2010). We have chosen

four upwellings – Atla, Beta, West Eistla and Themis Regio. In order to compare the observed rises with the axially symmetric ones in 2D models, we average the observed anomalies to get an axisymmetric shape.

Model setup

In our 3D models viscosity only varies with depth. Besides the viscosity profile A based on Pauer et al. (2006) we also use three simple viscosity stratifications: constant viscosity mantle (B), model C with linearly increasing viscosity and model D with a high a viscosity lithosphere underlain by an isoviscous mantle (Fig. 1). In 2D models the viscosity can also vary laterally through its temperature dependence:

$$\eta = \eta_{UM}\eta'(r)\exp\left[-\ln c\,\frac{T - T_{ref}}{T_{cmb} - T_{top}}\right]. \qquad (9)$$

Here η_{UM} is a constant (its choice controls the Ra), $\eta' = \eta'(r)$ is a dimensionless reference viscosity at radius r, T_{ref} is the reference temperature and c is a non-dimensional parameter that controls an additional temperature induced viscosity contrast between the top and bottom surfaces. For the values of the used parameters see Table 2.

As the observed data we use the model of the Venus' geoid by Konopliv et al. (1999) and the topography model by Rappaport et al. (1999).

Results

Though the geoid undulations are only dependent on the radial variations of the viscosity and not on its absolute value, the latter one defines the Rayleigh number and thus the convection vigour and the character of the density anomalies. Therefore, it affects the geoid considerably. We varied the upper mantle viscosity η_{UM} in the range $8 \cdot 10^{20} - 1 \cdot 10^{23}$ Pa s while holding other parameters fixed, so changing Rayleigh number in the range $9 \cdot 10^4 - 2.6 \cdot 10^7$. The spectra are sensitive to the upper mantle viscosity (Rayleigh number) and the preferred value of Rayleigh number is usually found around 10^6 (η_{UM} varies between 10^{21} and 10^{22} Pa s). For each viscosity profile (A - D) we thus obtain one model with best fit. In case of the viscosity profile A, the best fit is obtained for a model 3A2 $\times 10^{21}$ with the upper mantle viscosity η_{UM} $= 2 \cdot 10^{21}$ Pa s (average Ra $= 3 \cdot 10^6$). The best fitting constant viscosity model 3B4 $\times 10^{22}$ has $\eta_{UM} = 4 \cdot 10^{22}$ Pa s (Ra $= 3 \cdot 10^6$). Linearly increasing viscosity (model 3C5 $\times 10^{21}$) produces the best fit for the $\eta_{UM} = 5 \cdot 10^{21}$ Pa s (average Ra $= 6 \cdot 10^5$). Finally profile D with a stiff lithosphere prefers

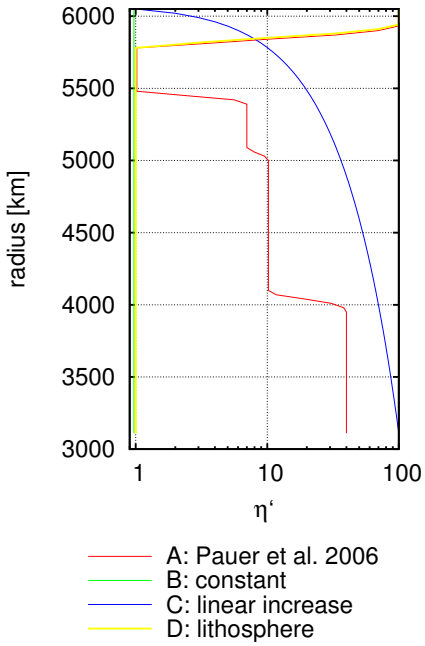

Figure 1: Four profiles of the radially dependent dimensionless viscosity $\eta^{'}(r)$ (cf. eq. (9)).

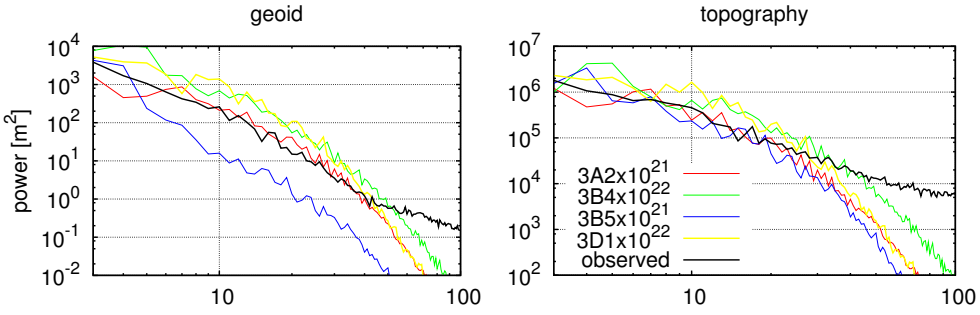

Figure 2: Power spectra of the geoid and topography of Venus. The results for four different viscosity profiles—each for its ideal Ra. Black line shows the spectrum of the observed data.

Table 2: Model parameters for Venus (Schubert et al., 2001; Yoshida and Kageyama, 2006)

Parameter	Symbol	Value	Units
radius of Venus	r_{top}	6050	km
core radius	r_{cmb}	3110	km
gravity acceleration	g	8.6	m s^{-2}
reference density	ρ_0	4200	kg m^{-3}
coefficient of thermal expansion	α	$2.5 \cdot 10^{-5}$	K^{-1}
specific heat at constant pressure	c_p	1200	J kg^{-1} K^{-1}
thermal diffusivity	κ	$5 \cdot 10^{-7}$	$m^2 s^{-1}$
density at the surface	$\Delta\rho_{top}$	3200	kg m^{-3}
density contrast at CMB	$\Delta\rho_{cmb}$	4300	kg m^{-3}
density of the core	ρ_{core}	12500	kg m^{-3}
temperature on the surface	T_{top}	731	K
temperature on the core-mantle boundary	T_{cmb}	3700	K
reference temperature	T_{ref}	2215	K
gravitational constant	G	$6.67 \cdot 10^{-11}$	N m^2 kg^{-2}
rate of internal heating	Q_v	$7.5 \cdot 10^{-9}$	W m^{-3}
Clapeyron slope	γ	$-2.8 \cdot 10^6$	Pa K^{-1}
density jump at 730 km	$\Delta\rho_{730}$	390	kg m^{-3}

the upper mantle viscosity of $\eta_{UM} = 1 \cdot 10^{22}$ Pa s with average Ra $= 1 \cdot 10^6$ (model 3D1$\times 10^{22}$).

Fig. 2 shows the geoid and topography spectra of best fitting models for each viscosity profile (A–D). Black line gives the spectra of the observed quantities. Clearly, as for the geoid, the best fitting model is A that explains the the observed data at degrees 5-40 very well. In the case of topography both models A and C correspond with data quite well up to degreee 20. Above degree 40 the predicted spectral slope does not correspond for any model.

One representation of the convection planform for each of the four above mentioned models is shown in Fig. 3 (each of them for the same time instant as the spectra in Fig. 2). The model 3D1$\times 10^{22}$ with the constant viscosity under the stiff lithosphere (Fig. 2d) has a rather warm mantle and thus is characterised by a vigorous plume activity, with the total number of plumes of about 30. That is probably too much — there should be about 10 major plumes on Venus (Smrekar and Parmentier, 1996; Smrekar et al., 2010).

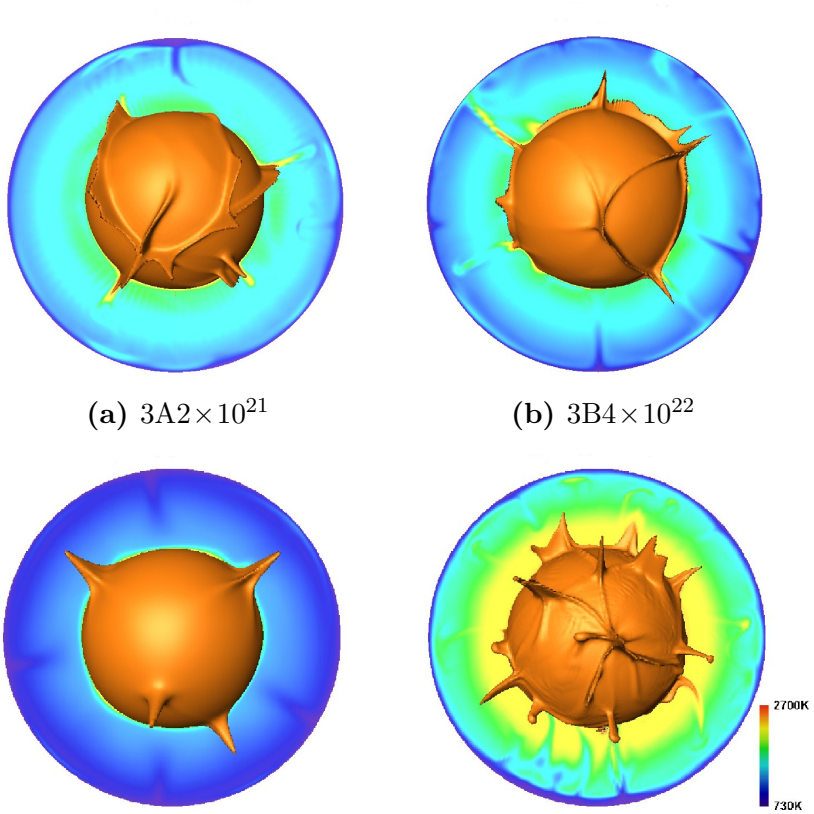

(a) 3A2$\times 10^{21}$ **(b)** 3B4$\times 10^{22}$

(c) 3C5$\times 10^{21}$ **(d)** 3D1$\times 10^{22}$

Figure 3: One snapshot of the temperature field in four convection models: a) viscosity profile A ($3A2 \times 10^{21}$), b) profile B ($3B4 \times 10^{22}$), c) profile C ($3C5 \times 10^{21}$) and d) profile D ($3D1 \times 10^{22}$) for their ideal Ra.

Models A–C are generally in agreement with that criterion.

Besides the power spectra of the geoid and the topography we used the actual shape of the geoid and topography above the assumed mantle plumes to discriminate between the successful and unsuccessful models. We use here the data in four upwelling areas (Atla, Beta, West Eistla and Themis) and compare the shape of the anomalies with the topography and the geoid predicted in the polar plume area in our axisymmetric model. Although the fit is poor for the most time instants, at certain moments, however, the error drops and a quite good fit is observed. It is difficult to identify a really successful model here as the moments with good fit are quite rare in all models, but again model A may be considered the best. The comparison between predicted and observed data is shown in Fig. 4. We should note here though, that the correspondence between the observed and predicted

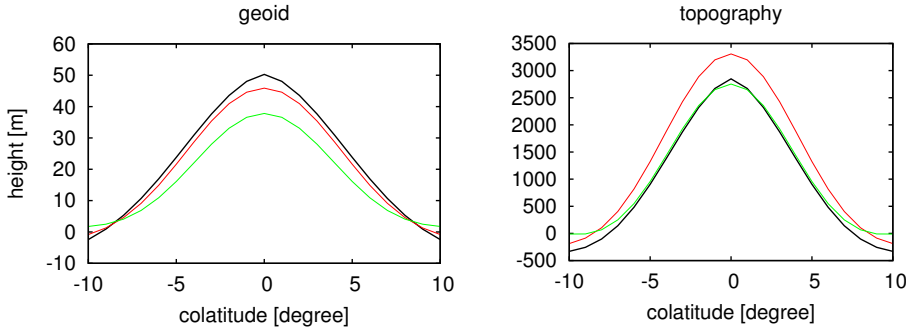

Figure 4: Observed geoid and topography in Atla Regio (black line) with the model prediction (model 2A2x10^{21}IH). Green and red lines give the predictions in two different snapshots. Geoid and topography are calculated for degrees 10-40.

topography and geoid differs among the considered Regia. Our models are more successful in explaining these quantities in Atla and Beta Regia, while for Western Eistla and Themis the fit is considerably lower.

Concluding Remarks

On the basis of combined evidence coming from the spectral geoid and topography fit, number of plumes developed in the mantle and the fit to the observed shape of the geoid and topography in several Regios on Venus, the profile A characterised by a 200 km thick lithosphere followed by a gradual increase of viscosity with depth gives the best correspondence between the observed and predicted quantities. The best fitting model has the upper mantle viscosity of $2{\cdot}10^{21}$ Pa s, thus giving an average Rayleigh number of $2.8 \cdot 10^6$. Both 2D and 3D model runs prefer the same upper mantle viscosity. That may suggest, that the plumes are indeed the main dynamic features controlling the dynamic processes in the Venus' mantle and the 2D axisymmetric model provides its good approximation. For all viscosity profiles the observed and predicted spectra coincide only up to the degree about 40. At higher degrees the slope of the predicted spectra differs from the observed ones considerably thus indicating other then dynamic origin of the geoid and topography anomalies.

The results of the presented 3D models are inevitably negatively influenced by the absence of the lateral variations of viscosity. However, it has been shown by Solomatov and Moresi (1996), that under the high viscosity stagnant lid the temperature variations are rather small and therefore also the temperature induced lateral variations of viscosity may not play a key

role. That is in a good agreement with the results of 2D models, where the moderate temperature related lateral variations of viscosity do not improve the fit to the data. Further, Tackley (1996) pointed out, that the depth viscosity variations play primary role in influencing the dynamic regime of the mantle. Thus, 3D results for a model with a high viscosity lid should be able to describe the basic features of the Venus mantle dynamics.

The similar analysis is also presented for Mercury.

Part II: Influence of the Post-Perovskite Phase on the Thermal Evolution of the Earth

Thermal evolution of the Earth mantle has been addressed in past decades in terms of volume averaged or parameterised models and recently also in fully dynamical simulations of convection. Numerous studies focused on various phenomena that affect cooling of the Earth mantle (e.g. van den Berg et al., 2004; Nakagawa and Tackley, 2005; Korenaga, 2010) and through the core-mantle coupling also the core evolution and magnetic field generation.

A new phenomenon that could potentially influence core-mantle coupling and cooling of the Earth appeared in 2004. Discovery of post-perovskite (PPV) (Murakami et al., 2004) motivated many studies that investigated its effects on the mantle convection. This exothermic phase transition has high Clapeyron slope — its value was estimated between 8 MPa/K and 13 MPa/K — but a small density contrast of 1%. High Clapeyron slope results in strongly variable depth of the PPV transition and, with higher core-mantle boundary (CMB) temperatures, double-crossing of this phase boundary occurs and isolated lenses of PPV are formed (Nakagawa and Tackley, 2005; Monnereau and Yuen, 2007).

In the early Earth, mantle was probably too hot to allow for the PPV formation. During mantle cooling PPV appeared at certain moment and may have exerted potentially strong effects on mantle evolution by increasing core-mantle heat flux and thus enhancing core cooling. Some of these effects have already been discussed also in terms of long-term models. Model of mantle thermal evolution and associated core cooling and inner-core growth of Nakagawa and Tackley (2010) included PPV phase transition, but did not take into account low viscosity PPV. They report weak dependence of the system on the initial CMB temperature and strong dependence on the chemical contrast in the deep mantle. Dense piles accumulated at the CMB facilitate obtaining correct final inner core size and maintaining geodynamo. Weak sensitivity to initial CMB temperature was confirmed in Nakagawa

and Tackley (2012), where magmatism was identified as dominant mechanism of heat loss in early stages of Earth evolution. Finally, Nakagawa and Tackley (2011) concentrated on the effect of weak PPV and concluded that it increases lateral extent of chemical anomalies and reduces CMB topography by weakening the slabs at the base of the mantle. As already pointed out before, it also increases CMB heat flux and should therefore potentially influence the rate of core cooling. Core cooling was however not included in their model.

Here we supplement these previous studies by investigating effects of rheologically distinct post-perovskite on the mantle cooling in the model that includes decaying heat sources and heat extraction from the core. Core is assumed to be an isothermal heat reservoir with temperature controlled by heat flux through CMB. We simulate long-term evolution of the mantle from hot initial state and we evaluate combined effects of weak post-perovskite and several other parameters (thermal expansivity, diffusivity, initial core temperature).

Model setup

We performed the calculations in 2D axisymmetric model. We use two models of internal heating rate and its time decay. Model MH1 assumes equation

$$H(t) = \sum_{i=U,Th,K} H_0^i \, \exp\left(-\frac{t \ln 2}{\tau^i}\right), \tag{10}$$

where initial productions of individual radioactive elements H_0^i are calculated from their present-day values and half-lives τ^i (Lowrie, 2007). Second model of internal heating MH2 follows relation

$$H(t) = \frac{1}{M}\Big((10.26t + 51.16)\exp(-t) - 2.49t + 26.78\Big), \tag{11}$$

where $M = 3.63216 \cdot 10^{24}$ kg is the mass of the Earth. This formula was interpolated from van Schmus (1995).

Heat extracted from the core during long-term cooling should be reflected in decreasing CMB temperature T_{cmb}. In our model the core is considered to be an isothermal heat reservoir and its temperature T_C is controlled by the total heat flux through core-mantle boundary Q_{cmb} (van den Berg et al., 2005):

$$\frac{\mathrm{d}T_C}{\mathrm{d}t} = -\frac{Q_{cmb}(t)}{\varrho_C \, c_{pC} \, V_C}. \tag{12}$$

Here ϱ_C is the density of the core, c_{pC} is the specific heat of the core at constant pressure and V_C is the volume of the core. The term $\varrho_C c_{pC} V_C$ is the total heat capacity of the core.

Viscosity depends on pressure (through radius r) and temperature following formula

$$\eta(r,T) = \Delta\eta\,\eta_0 \exp\left[a\frac{r_{top}-r}{r_{top}-r_{cmb}} - b\frac{T-T_{top}}{T_{cmb}-T_{top}}\right]. \qquad (13)$$

An arbitrarily chosen parameter η_0 controls Rayleigh number, $a = 4.6052$ m^{-1} results in two orders of magnitude viscosity increase with depth while $b = 5.0106$ K^{-1} determines temperature variations of viscosity of the order of 150. As this temperature dependence is relatively weak we apply additional viscosity contrast $\Delta\eta$ which is depth dependent. In uppermost 100 km of the model $\Delta\eta = 10$ to produce stronger lithosphere. In the rest of the mantle $\Delta\eta = 1$. Additional viscosity variations are introduced due to phase transitions.

All models include the spinel-perovskite endothermic phase transition at 660-km depth. In some models, perovskite to PPV exothermic transition is prescribed. PPV phase is either by one or two orders of magnitude weaker than perovskite at the same pressure and temperature conditions. In these model cases viscosity according to formula (13) is multiplied by a factor $\Delta\eta_{ppv} = 0.1$ or 0.01 within the PPV stability area. Phase transition at 660-km depth is associated with viscosity increase by a factor $\Delta\eta_{660} = 10$.

Thermal conductivity is either constant k_0 or radially-dependent. The model of radially dependent $k(r)$ based on pressure and temperature dependent model of Hofmeister (1999) is taken from van den Berg et al. (2005). Thermal expansivity is either constant α_0 or radially dependent (Matyska et al., 2011).

Parameters used in our study are summarised in Table 3. We performed series of 2D axisymmetric model runs with initial average $Ra = 10^6$ and 10^7 and varying parameters.

Results

Fig. 5 shows results of models with lower initial $Ra = 10^6$ with constant expansivity and diffusivity. Cooling of the Earth in reference model without weak PPV is shown in Fig. 5a. Here time evolution of temperature is plotted in four snapshots. In the first snapshot mantle is hot with four plumes rising from the CMB region. Some of the cold downwellings are hindered at the 660-km boundary due to the combined effects of endothermic phase transition and viscosity increase. Both mantle and core are cooling with time, tendency to

Parameter	Symbol	Value	Units
radius of the Earth	r_{top}	6371	km
core radius	r_{cmb}	3471	km
gravity acceleration	g	9.87	m s^{-2}
reference density	ρ_0	4000	kg m^{-3}
specific heat at constant pressure	c_p	1250	J kg^{-1} K^{-1}
thermal expansivity	α_0	$2.5 \cdot 10^{-5}$	K^{-1}
thermal conductivity	k_0	5.9	W m^{-1} K^{-1}
density of the core	ϱ_C	12500	kg m^{-3}
specific heat of the core	c_{pC}	500	J kg^{-1} K^{-1}
temperature on the surface	T_{top}	273	K
Clapeyron slope (660 km)	γ_{660}	-2.5	MPa K^{-1}
density jump (660km)	$\delta\rho_{660}$	342	kg m^{-3}
width of the 660 km transition	d_{660}^{ph}	40	km
relative viscosity change	$\Delta\eta_{660}$	10	
Clapeyron slope of ppv phase transition	γ_{ppv}	10	MPa K^{-1}
density jump at ppv phase transition	$\Delta\rho_{ppv}$	40	kg m^{-3}
temperature intercept	T_{int}	3800	K
width of ppv phase transition	d_{ppv}^{ph}	200	km
relative viscosity change	$\delta\eta_{ppv}$	1, 0.1, 0.01	

Table 3: Model parameters

layered flow pattern is decreasing and in the final snapshot most downwellings reach lower mantle, though some of them are temporarily deflected at 660-km interface. The evolution of core temperature is demonstrated in Fig. 6 (left) (red curve). Core cooling is ineffective in the first 0.5 Ga, mainly due to the 660-km phase transition. In the hot early mantle this phase transition enforces layered flow and the overheated lower mantle is blanketing core and reducing core cooling. CMB heat flux is decreasing (Fig. 6, right) and very short periods of negative heat flux may even appear when core is temporarily warming. After this initial period, phase transition effects are getting weaker, as mantle is cooling and Ra decreasing. CMB heat flux increases and core temperature is decreasing steadily.

If PPV weaker by one order of magnitude is taken into account we observe some changes in character of flow (Fig. 5b). PPV first appears in the coldest material above CMB at about 0.5 Ga after the initial state. Weakening of the cold foot of the slab results in enhanced lateral flow above the CMB and consequently the downwellings are thinner than in case without bottom

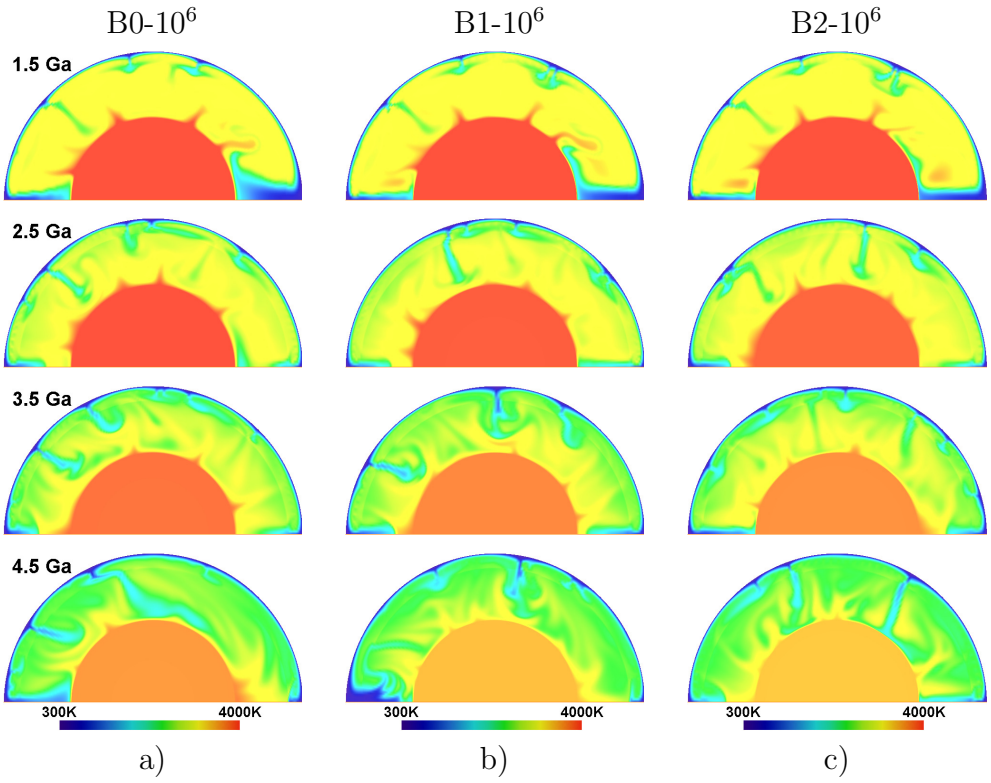

Figure 5: Models B-10^6: time evolution of temperature

weakening. Higher mobility of cold material in the bottom boundary layer increases CMB heat flux (Fig. 6, right, green curve) and makes core cooling more efficient (Fig. 6, left, green curve). Resulting core temperature is thus by 150 K lower than in model without weak PPV. Yet lower PPV viscosity (model B2-10^6, Fig. 5c) further enhances CMB heat flux, especially in the time intervals when massive cold downwellings arrive at the CMB. Resulting CMB temperature is thus by about 30 K lower than in case of intermediate PPV viscosity (Fig. 5a).

Except of PPV viscosity, there are apparently some other model parameters that affect cooling efficiency. We further evaluated effects of some of them, namely initial core temperature, depth-dependent thermal conductivity, internal heating rate, depth-dependent thermal expansivity and combination of these. Model with higher initial CMB temperature results in rather similar flow pattern as reference model B0-10^6, though the average mantle temperature is somewhat higher than in reference case. Also higher initial internal heating rate produces final state with slightly higher average mantle temperature thanks to the fact that cooling rate in the initial 1 Ga

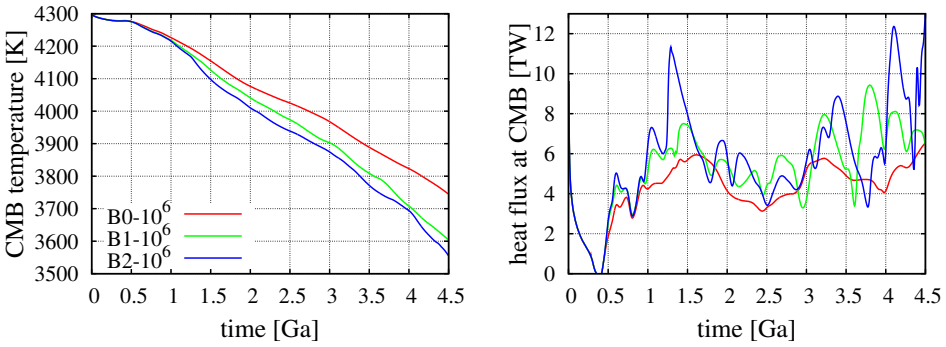

Figure 6: Models B-10^6: time evolution of core-mantle boundary temperature, and heat flux at the core-mantle boundary. B0-10^6 is the reference model without PPV phase, B1-10^6 and B2-10^6 models account for 1 or 2 orders of magnitude weaker PPV.

is much less efficient than in reference case. Much more pronounced effect to mantle temperature is however observed in model with depth-dependent conductivity. Here relatively low conductivity at shallow depths suppresses heat extraction from the mantle and results in significantly higher mantle temperatures. Warmer mantle is in turn less efficient in extracting heat from the core and the final CMB temperature is thus by about 100 K higher than in reference case. Finally, thermal expansivity decreasing with depth results in long-wavelength lower-mantle downwellings and sluggish convection that is significantly less efficient in removing heat from the core. Both average mantle temperature and CMB temperature are thus higher than in reference model. Combination of depth-dependent expansivity and conductivity is further studied. Both parameters tend to stabilize lower-mantle circulation and result in relatively slow long-wavelength flow and consequently in significantly warmer mantle and core. Endothermic phase transition at 660-km depth acts as a more effective barrier in these models and we observe partially layered convection that is so inefficient in removing heat from the lower mantle, that average mantle temperature is increasing within first 1.5 Ga of mantle evolution.

Finally, we evaluated the effects of higher initial $Ra = 10^7$. We uses the model with combined effects of depth-dependent parameters $k(r)$ and $\alpha(r)$ and higher initial CMB temperature. Temperature in the last snapshot of simulation is shown in Fig. 7. Weak PPV in combination with depth-dependent properties clearly have much stronger effect in this more vigorous convection model with depth-dependent parameters. Endothermic phase transition at 660-km now enforces partially layered convection. PPV first

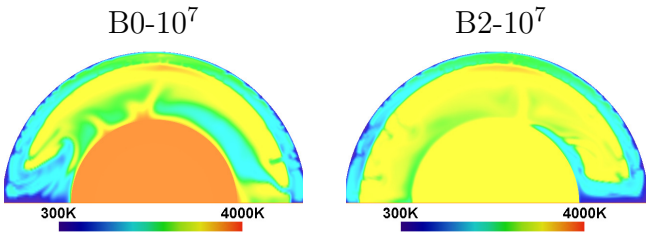

Figure 7: Snapshot of temperature taken at 4.5 Ga for models B-10^7. B0-10^6 is the model without PPV phase and B2-10^6 model accounts for 2 orders of magnitude weaker PPV.

appears in the model after 1 Ga evolution from the initial state in sporadic isolated patches (Fig. 8a) — earlier than in a corresponding model with lower $Ra = 10^6$. These patches are caused by an avalanche of cold upper mantle material penetrating 660-km boundary and arriving at the CMB. Presence of weak PPV is reflected in increased CMB heat flux (Fig. 8b) and somewhat enhanced core cooling (Fig. 8d). PPV then temporarily disappears and until 2.5 Ga plays hardly any role. At 2.5 Ga next massive avalanche of cold material cools lowermost mantle and since that moment PPV lenses are present as indicated in Fig. 8a, where average PPV thickness is plotted as a function of time. Since then CMB heat flux is strongly enhanced (Fig. 8b) and core cooling is much more efficient (Fig. 8d). Final core temperature is thus by more than 400 K lower than in case without weak PPV and average mantle temperature is by about 70 K higher (Fig. 8c). Vigorous convection of higher Ra models is much more efficient in removing heat from the lower mantle and we therefore do not observe here temporary increase of mantle temperature (Fig. 8c).

Concluding remarks

In agreement with previous studies (e.g. Nakagawa and Tackley, 2011) we show that weak post-perovskite in the bottom thermal boundary layer tends to destabilize flow and enhance convective vigour. While the effects of weak post-perovskite on the average mantle temperature are rather small ($\sim$ 100 K) the resulting core temperature may be by more than 400 K lower if post-perovskite is taken into account. Weak post-perovskite further enhances CMB heat flux (Nakagawa and Tackley, 2011; Li et al., 2014). Heat flux variations with time reflect episodes of massive cold downwellings arriving at the CMB associated with post-perovskite formation. Such episodic heat flux variations may be required to induce changes in geodynamo reversal behaviour (Biggin et al., 2012).

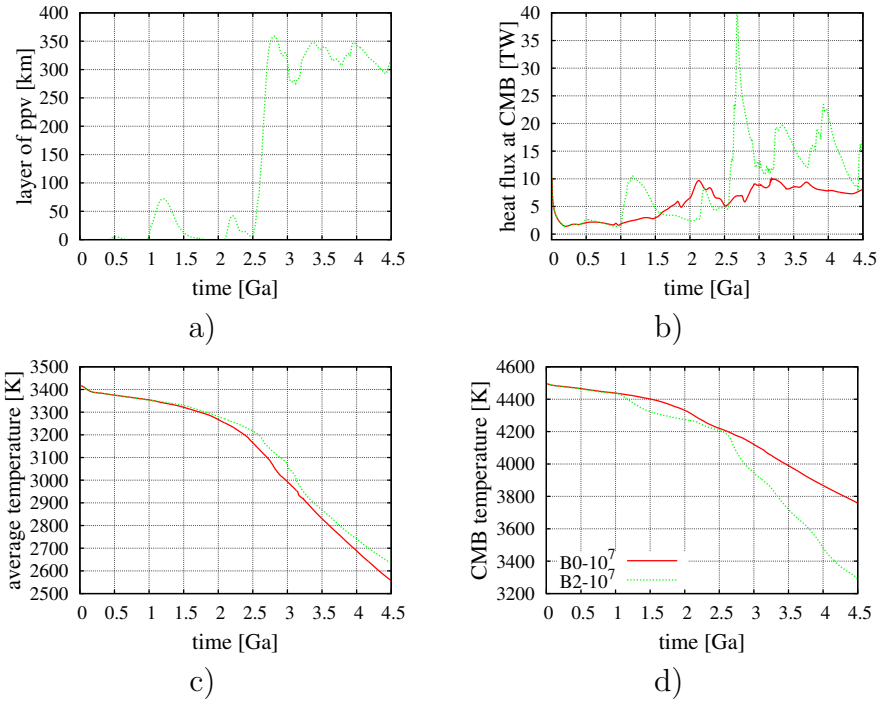

Figure 8: Models B-10^7: time evolution of selected quantities.

van den Berg et al. (2005) studied effects of thermal conductivity on mantle thermal evolution and concentrated on contributions from both phonon and radiative components of conductivity (Hofmeister (1999)). They report that temperature and pressure dependent phonon conductivity delays cooling thanks to relatively low conductivity at shallow depths, while radiative contribution that increases lowermost mantle conductivity supports heat extraction from the core and enhances cooling. Here we also observe that including depth-dependent conductivity and expansivity in the models with lower Ra and without weak PPV increases average mantle temperature and delays secular cooling through formation of less conductive layer in the uppermost mantle and through less vigorous flow in the lower mantle. Weak post-perovskite has only mild effects on the average mantle temperature, it however significantly affects resulting core temperature and heat flux.

Conclusions

In this thesis, we addressed several questions concerning mantle convection in the terrestrial bodies. We developed and tested the code for numerical simulations of mantle convection in 2D axisymmetric and 3D spherical geometry

and applied it to problems related to Earth, Venus and Mercury thermal evolution.

We concentrated on three main issues: i) constraining viscosity structure of Venus using its gravity and topography data, ii) finding out whether Mercury geoid and topography could be supported by mantle convection and iii) evaluating the effects of rheologically distinct post-perovskite on secular cooling of the Earth.

In the first part, we tried to extend knowledge of the structure and dynamics of the Venusian mantle. We performed a search for the viscosity and density models that would most closely fit the spectra of observed geoid and dynamic topography. We selected four possible radial viscosity profiles and for each of them we generated a broad group of models with varying Rayleigh number (that controls the character of thermally induced density anomalies) and with weaker or stronger lateral variations of viscosity. Further, we monitored the topography and the geoid developing above individual plumes and compared them with the observed elevations of Venus' geoid and topography in several Regii. We conclude that the best fitting viscosity profile is characterised by the upper mantle viscosity of $2{\cdot}10^{21}$ Pa s, with a strong 200 km thick lithosphere, without an asthenosphere and with a gradual viscosity increase in the underlying mantle. Lateral variations of viscosity play only a minor role and do not significantly improve the fit. Our models predict the observed spectra well only up to the degree of about 40 thus indicating other then dynamic origin of the geoid and topography anomalies for higher degrees.

Similar analysis applied to Mercury employed recent measurements of MESSENGER mission. We assumed that Mercurian mantle is currently still convecting and we tried to predict the spectra of its geoid and topography in terms of our convection models. Contrary to the above summarised results for Venus, we were not able to predict the observed geoid and topography. This negative result is in agreement with recently published analysis of geoid and topography data, that suggests other mechanisms to be important, namely variations of crustal thickness and (possibly compositional) deep mantle anomalies. It also provides an indirect indication that perhaps Mercurian mantle convection already ceased as suggested by several authors.

Last part of the thesis is focused on the effects of PPV in the Earth mantle convection and on its spatial distribution. Simulations of a long-term evolution of the mantle take into account decaying radiogenic heat sources, variable material properties and thermal coupling between the mantle and the core. We conclude that weak PPV in the bottom thermal boundary layer tends to destabilize flow, increase convective vigour and enhance CMB heat flux. This results in a considerably lower CMB temperature, but the effect

on the average mantle temperature is small. On the other hand, while presence of weak PPV enhances the secular cooling, depth-dependent material parameters (thermal expansivity and diffusivity) tend to delay the secular cooling.

Finally, thermal structures produced in our numerical models were used in the synthetic inversion of EM data that tried to determine possible detectability of highly conductive PPV lenses. PPV distribution obtained in our 3D thermal convection models was used as one possible synthetic input for EM inversion. Results suggest that highly conductive PPV is only visible if its spatial distribution is interconnected in the equatorial direction. Isolated conductive PPV lenses resulting from our convection simulations could not be detected by 1D EM inversion. The fact that 1D inversion of real data did not detect highly conductive layer at the base of the mantle thus indicates that PPV is probably indeed present there in isolated patches rather than in a continuous layer.

References

ARMANN, M. and TACKLEY, P. J. 3-D Spherical Modelling of the Thermo-Chemical Evolution of Venus' Mantle and Crust. In *EGU General Assembly Conference Abstracts*, 12, p. 10507, May 2010.

BIGGIN, A. J. et al. Possible links between long-term geomagnetic variations and whole-mantle convection processes. *Nature Geosci.* 2012, 5, 9, pp. 674.

ČÍŽKOVÁ, H. and ČADEK, O. Effect of a Viscosity Interface at 1000 km Depth on Mantle Circulation. *Stud. Geophys. Geod.* 1997, 41, pp. 297–306.

HOFMEISTER, A. M. Mantle Values of Thermal Conductivity and the Geotherm from Phonon Lifetimes. *Science.* 1999, 283, 5408, pp. 1699–1706.

ITA, J. and KING, S. D. Sensitivity of convection with an endothermic phase change to the form of governing equations, initial conditions, boundary conditions, and equation of state. *J. Geophys. Res.* 1994, 99, B8, pp. 15919–15938.

KIEFER, W. S. and HAGER, B. H. A mantle plume model for the Equatorial Highlands of Venus. *J. Geophys. Res.* 1991, 96, E4, pp. 20947–20966.

KING, S. et al. A Community Benchmark for 2D Cartesian Compressible Convection in th Earth's Mantle. *Geophys. J. Int.* 2010, 180, pp. 73–87.

KONOPLIV, A. S., BANERDT, W. B. and SJOGREN, W. L. Venus gravity: 180th degree and order model. *Icarus.* 1999, 139, pp. 3–18.

KORENAGA, J. Scaling of plate tectonic convection with pseudoplastic rheology. *J. Geophys. Res.-Sol. Ea.* 2010, 115, B11.

LI, Y., DESCHAMPS, F. and TACKLEY, P. J. Effects of low-viscosity post-perovskite on the stability and structure of primordial reservoirs in the lower mantle. *Geophys. Res. Lett.* 2014, 41, 20, pp. 7089–7097.

LOWRIE, W. *Fundamentals of Geophysics*. Cambridge University Press, 2007.

MATYSKA, C. and YUEN, D. Lower mantle material properties and convection models of multiscale plumes. In FOULGER, G. and JURDY, D. (Ed.) *Plates, plumes, and planetary processes: Geological Society of America Special Paper 430*. The Geological Society of America, 2007. pp. 137–163.

MATYSKA, C. et al. The impact of variability in the rheological activation parameters on lower-mantle viscosity stratification and its dynamics. *Phys. Earth Planet. In.* 2011, 188, 1–2, pp. 1 – 8.

MONNEREAU, M. and YUEN, D. A. Topology of the postperovskite phase transition and mantle dynamics. *P. Natl. Acad. Sci. USA*. 2007, 104, 22, pp. 9156–61.

MURAKAMI, M. et al. Post-Perovskite Phase Transition in $MgSiO_3$. *Science*. 2004, 304, 5672, pp. 855–858.

NAKAGAWA, T. and TACKLEY, P. J. The interaction between the post-perovskite phase change and a thermo-chemical boundary layer near the core–mantle boundary. *Earth Planet. Sci. Lett.* 2005, 238, 1–2, pp. 204 – 216.

NAKAGAWA, T. and TACKLEY, P. J. Influence of initial CMB temperature and other parameters on the thermal evolution of Earth's core resulting from thermochemical spherical mantle convection. *Geochem. Geophys. Geosyst.* 2010, 11, pp. Q06001.

NAKAGAWA, T. and TACKLEY, P. J. Effects of low-viscosity post-perovskite on thermo-chemical mantle convection in a 3-D spherical shell. *Geophys. Res. Lett.* 2011, 38, pp. L04309.

NAKAGAWA, T. and TACKLEY, P. J. Three-dimensional structures and dynamics in the deep mantle: Effects of post-perovskite phase change and deep mantle layering. *Geophys. Res. Lett.* 2012, 33, pp. L12S11.

PAUER, M., FLEMING, K. and ČADEK, O. Modeling the dynamic component of the geoid and topography of Venus. *J. Geophys. Res.* 2006, 111, E11.

RAPPAPORT, N. J. et al. An Improved 360 Degree and Order Model of Venus Topography. *Icarus*. 1999, 139, 1, pp. 19 – 31.

SCHUBERT, G., TURCOTTE, D. L. and P., O. *Mantle Convection in the Earth and Planets*. New York : Cambridge Univ. Press, 2001.

SMREKAR, S. E. et al. Recent Hotspot Volcanism on Venus from VIRTIS Emissivity Data. *Science*. 2010, 328, 5978, pp. 605 – 608.

SMREKAR, S. E. and PARMENTIER, E. M. The interaction of mantle plumes with surface thermal and chemical boundary layers: Applications to hotspots on Venus. *J. Geophys. Res.* 1996, 101, B3, pp. 5397 – 5410.

SOLOMATOV, V. S. and MORESI, L.-N. Stagnant lid convection on Venus. *J. Geophys. Res.* 1996, 101, pp. 4737–4753.

STOFAN, E. R. and SMREKAR, S. E. Large topographic rises, coronae, large flow fields, and large volcanoes on Venus: Evidence for mantle plumes? In FOULGER, G. and JURDY, D. (Ed.) *Plates, Plumes, and Planetary Processes*. Geological Society of America Special Paper 338, 2005. pp. 841–861.

TACKLEY, P. J. Effects of strongly temperature-dependent viscosity on time-dependent, 3-dimensional models of mantle convection. *Geophys. Res. Lett.* 1993, 20.

TACKLEY, P. J. Effects of strongly variable viscosity on three-dimensional compressible convection in planetary mantles. *J. Geophys. Res.* 1996, 101.

van den BERG, A. P., YUEN, D. and RAINEY, E. The influence of variable viscosity on delayed cooling due to variable thermal conductivity. *Phys. Earth Planet. In.* 2004, 142, 3–4, pp. 283 – 295.

van den BERG, A. P., RAINEY, E. G. and YUEN, D. The combined influences of variable thermal conductivity, temperature- and pressure-dependent viscosity and core–mantle coupling on thermal evolution. *Phys. Earth Planet. In.* 2005, 149, 3–4, pp. 259 – 278.

van HUNEN, J. *Shallow and buoyant lithospheric subduction: causes and implications from thermo-chemical numerical modeling*. PhD thesis, Utrecht University, 2001.

van SCHMUS, W. R. Natural radioactivity of the crust and mantle. In AHRENS, T. J. (Ed.) *Global Earth Physics: A Handbook of Physical Constants*. AGU, 1995. pp. 283–291.

YOSHIDA, M. and KAGEYAMA, A. Low-degree mantle convection with strongly temperature- and depth-dependent viscosity in a three-dimensional spherical shell. *J. Geophys. Res.* 2006, 111, B3.

Author's publications and citation report

- BENEŠOVÁ, N. and ČÍŽKOVÁ, H. Geoid and topography of Venus in various thermal convection models. *Stud. Geophys. Geod.* 2012, 56, 2, pp. 621—639.
    - ORTH, C. P. and SOLOMATOV, V. S., Constraints on the Venusian crustal thickness variations in the isostatic stagnant lid approximation. *Geochem. Geophys. Geosyst.* 2012, 13, 11, pp. 1525–2027.
    - DUMOULIN, C., ČADEK, O. and CHOBLET, G., Predicting surface dynamic topographies of stagnant lid planetary bodies. *Geophys. J. Int.* 2013, 195, 3, pp. 1494–1508.
- VELÍMSKÝ, J., BENEŠOVÁ, N. and ČÍŽKOVÁ, H., On the detectability of 3-D postperovskite distribution in D" by electromagnetic induction. *Phys. Earth Planet. In.* 2012, 202–203, pp. 71–77.
    - PLOTKIN, V. V., DYAD'KOV, P. G., and OVCHINNIKOV, S. G., Detecting a magnesiowüstite phase transition in the lower mantle by inversion of geomagnetic data. *Russ. Geol. Geophys.* 2014, 55, 9, pp. 1138–1145.
    - JAULT, D., Illuminating the electrical conductivity of the lowermost mantle from below. *Geophys. J. Int.* 2015, 202, 1, pp. 482–496.
- BENEŠOVÁ, N. and ČÍŽKOVÁ, H. Effect of post-perovskite rheology on the thermal evolution of the Earth. *Submitted to Phys. Earth Planet. In.*